

RESEARCH ARTICLE

Efficient nanoparticle focusing utilizing cascade AC electroosmotic flow

Ahmed Abdelghany¹  | Keiichi Yamasaki¹ | Yoshiyasu Ichikawa^{1,2}  | Masahiro Motosuke^{1,2} 

¹Department of Mechanical Engineering, Tokyo University of Science, Tokyo, Japan

²Water Frontier Research Center, Research Institute for Science and Technology, Tokyo University of Science, Tokyo, Japan

Correspondence

Ahmed Abdelghany and Masahiro Motosuke, Department of Mechanical Engineering, Tokyo University of Science, 6-3-1 Nijjuku, Katsushika, Tokyo 125-8585, Japan.

Email: 4521701@ed.tus.ac.jp; mot@rs.tus.ac.jp

Color online: See article online to view Figures 1–7 in color.

Funding information

A part of this research was financially supported by Japan Society for the Promotion of Science (JSPS) KAKENHI, Grant/Award Numbers: 19H02084, 19K21936

Abstract

This study presents on-chip continuous accumulation and concentration of nanoscale samples using a cascade alternating current electroosmosis (cACEO) flow. ACEO can generate flow motion caused by ion movement due to interactions between the AC electric field and the induced charge layer on the electrode surface, with the potential to accumulate particles, especially in low-conductive liquid. However, the intrinsic particle diffusive motion, which is sensitive to particle size, is an essential element influencing accumulation efficiency. In this study, an electrode combining chevron and double-gap geometry embedded in a microfluidic channel was developed to perform efficient three-dimensional (3D) nanoparticle focusing using ACEO. The chevron electrode pattern was introduced upstream of the focusing zone to overcome particle accumulation in scattering zones near the channel sidewall. To demonstrate the efficiency of the proposed device for particle accumulation, three nanoparticle types were used: latex, metal, and biomaterial. Continuous 3D concentration of 50-nm polystyrene particles was confirmed. The concentration factor, determined based on image processing, became quite high when 50-nm gold nanoparticles were used. Moreover, nanoparticles with a 20-nm diameter were accumulated using cACEO. Finally, we used the concentrator chip to accumulate 50-nm liposome particles, confirming that the device could also successfully concentrate biomaterials.

KEYWORDS

cascade alternating-current electroosmotic flow, nanoparticles, particle accumulation

Abbreviations: 3D, three-dimensional.; ACEO, alternating current electroosmosis; AgNPs, silver nanoparticles; AuNPs, gold nanoparticles; cACEO, cascade alternating current electroosmosis; CF, concentration factor; CH, chevron; DG, double gap; ITO, indium tin oxide; PsNPs, polystyrene nanoparticles.

This is an open access article under the terms of the [Creative Commons Attribution-NonCommercial-NoDerivs](https://creativecommons.org/licenses/by-nc-nd/4.0/) License, which permits use and distribution in any medium, provided the original work is properly cited, the use is non-commercial and no modifications or adaptations are made.

© 2022 The Authors. *Electrophoresis* published by Wiley-VCH GmbH.

1 | INTRODUCTION

Microfluidic technology has gained a lot of attention in recent decades, and its application areas have grown to include biology, chemistry, life science, and engineering [1–3]. In this technology, precise manipulation of micro- and nanoparticles is essential for accumulating functional materials, enhancement or flexible control of surface reactions, and improved target material detection. Due to the intrinsically difficult detection in miniaturized devices, highly sensitive detection or analysis utilizing microfluidic devices have been the primary issues. The major causes include small sample volume or fluidic channels with a short optical path [4]. Enhancing detection sensitivity can be achieved by developing extremely sensitive detection techniques or achieving concentration before the analysis. As reported in previous studies [5, 6], preconcentration significantly improves the detection performance of rare samples in the reagent.

Numerous approaches for microfluidic particle focusing have been well established and frequently utilized to manipulate micro- and nanoparticles in a microfluidic device based on different forces, such as acoustic force [7, 8], optical forces [9], magnetic forces [10], and electrical forces [11–20]. However, the acoustic approach is ineffective for nanoparticles, because acoustic force is proportional to particle diameter. Moreover, optical methods are sometimes costly and challenging to utilize with nanoparticles. Furthermore, magnetic effects can be neglected in microstructures when compared to the electric field, since the energy stored in the magnetic field is significantly lower than the energy stored in the electrical field. Hence, electric forces are ideal for microfluidics, because they can produce a high field strength with low voltages across a wide frequency range [21].

Electrokinetics is a well-known phenomenon of particle transport in a solution in a microfluidic device due to the interaction between an electric field and a fluid or particle and can be achieved with a DC or AC field. It is used because microelectrode structure integration into microfluidic systems provides an opportunity to apply electrostatic force to the working fluid or solid colloid particles monodispersed inside [22, 23]. The AC electrokinetics approach has several advantages over DC-based techniques, such as electrophoresis, including a lower temperature rise owing to Joule heating, lower solution electrolysis, and less damage to target particles.

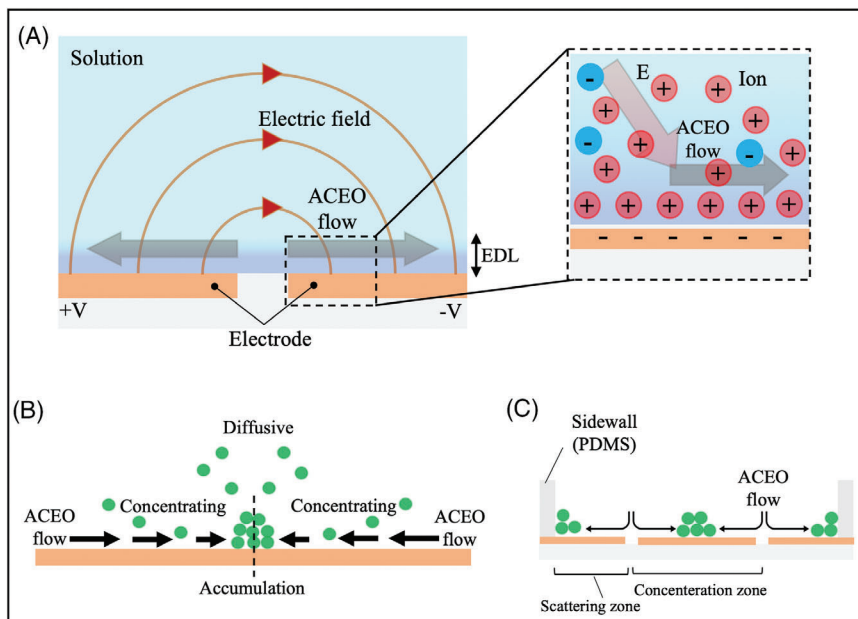
AC electrokinetics is an efficient approach for focusing particles, in which particles are driven through a microfluidic device and forces such as dielectrophoretic (DEP) or alternating current electroosmosis (ACEO) are applied to the particles, restricting them to a narrow stream [24, 25]. DEP methods frequently require complicated electrode

designs and a rigorous particle size limit. Furthermore, the DEP force is weak until a significant field gradient is produced [26]. On contrary, particle motion in the ACEO technique is independent of particle characteristics, because the particles are transported by a fluidic motion. As a result, ACEO has advantages in particle accumulation, particularly for submicron particles and nanoparticles [27–29].

In this study, we focused on the ACEO technique to accumulate nanoparticles. ACEO shows a field-induced fluid flow formed by an interaction between the electric double layer (EDL) and the tangential component of the electric field [30]. When an electric field is applied to electrode pairs, counterions of applied voltage create an induced charge layer, and the electrodes are capacitively charged. The counterions are movable and can migrate under the influence of an electric field tangential component, as illustrated in Figure 1A. The ACEO flow transports particles from the bulk of the fluid surface to the stagnation point of the fluid motion. Although DEP force should act on nanoparticles, especially near the electrode edge, we could not find trapped particles there. Therefore, DEP seems to exert a very weak effect. Furthermore, since ACEO flow is tangential over the electrode surface, delivered particles here are mainly affected by their spontaneous diffusion as a force normal to the surface. We thus suppose that particle transportation is effective as long as the ACEO convective motion outweighs the particle natural diffusive motion. Figure 1B depicts a schematic model of the focusing phenomenon. The particles are concentrated at the location where the advective force and diffusive behavior are balanced [24].

The ACEO flow carries particles in bulk to a high electric field area and then to a lower electric field area along the electrode surface. Under certain conditions, this unique flow behavior enables particles to concentrate at a specific spot in a microchannel with an electrode array. Earlier studies [28, 29, 31] investigated the efficiency of particle concentration by ACEO around electrodes placed at particular positions in the microchannel, confirming that the ACEO can accumulate particles toward a specific spot on the electrode depending on the electrode array design. The parallel double-gap (DG) electrode geometry allows the majority of the suspended particles to be collected at the center of the electrode. However, because of the nature of the ACEO flow, as indicated in Figure 1C, a dense area of particles is created at each side wall due to the counter-ACEO flow. Consequently, when using a DG electrode shape, a scattering area where particles are dispersed is unavoidable at the outside edges of the concentrating area. Therefore, implementing an additional scheme to control the initial particle position can reduce the number of particles flowing in the scattering zone

FIGURE 1 (A) Schematic diagram of alternating current electroosmosis (ACEO) caused by ion mobility in a diffusive layer exposed to an AC electric field. (B) Accumulation model based on the balance assumption. (C) Schematic diagram for concentration zone and scattering zone



and improve concentration performance, as discussed in our related work [32]. Using the concept of cascade electrodes, we were able to accumulate microscale particles for long-ranged concentration in a microfluidic channel with an overall concentration rate of nearly 98% for fluorescent polystyrene particles with a diameter of 0.5, 1.0, or 2.0 μm . The particle size does not affect the ACEO flow itself. However, for the particle accumulation using ACEO, as indicated in Figure 1B, the particle transportation is effective if the ACEO convective motion outweighs the diffusive motion of the particles, which is sensitive to particle size. It is difficult here to predict the effect of changing the particle size theoretically. Thus, we tried experimentally to investigate the applicability to accumulate submicron size particles using the same electrode configuration that was used in our previous study [32], an asymmetric electrode combined with the DG electrode. However, as the particle size decreased, the diffusive motion increased, and thus the accumulation performance also decreased. We found that to accumulate nanoparticles we need an electrode structure with a shorter periodic arrangement than the asymmetric electrode to minimize the effect of the diffusion.

To broaden the scope of particle concentration by ACEO flow to include rare sample detection, long-ranged nanoscale particle concentration along the streamwise direction in the flow channel must be verified. In this study, we present a new nanoparticle concentrator based on enhanced cascade ACEO (cACEO) that reduces applicable particle size to the nanoscopic domain and performs continuous nanoparticle concentration by three-dimensional (3D) flow configuration. A combination of

ACEO flow induced by a chevron (CH) electrode pattern upstream of the focusing zone and a DG electrode pattern in the focusing zone. The CH electrode was used to generate inward flow from the sidewall to the center area to accumulate particles from the scattering area efficiently; then, the DG electrode provides the necessary ACEO to concentrate nanoparticles effectively. Thus, the cACEO device was used to demonstrate the concentration efficiency of fluorescent latex nanoparticles, metal nanoparticles, and liposomes with a size range of 20–50 nm.

2 | MATERIALS AND METHODS

2.1 | Device structure and chip fabrication

The cACEO nanoparticle concentrator consists of two parts: a PDMS microfluidic channel and a glass substrate with two coplanar electrodes, as shown in Figure 2A. Electrode geometry is shown in Figure 2B. The CH electrode is located on the upstream side, while the DG electrode is located on the downstream side. The CH electrode has branches that generate inward flow from the sidewall to the center of the channel. The DG electrode induces the flow to concentrate nanoparticles in the center of the channel. The CH branches are 50- μm wide with a 25- μm space inclined at 30°. The DGs are 75 μm and are set parallel to the main flow direction. The center electrode in DG has a width of 200 μm , and each side electrode is 75- μm wide. For convenient fabrication, a 90-nm-thick indium tin oxide

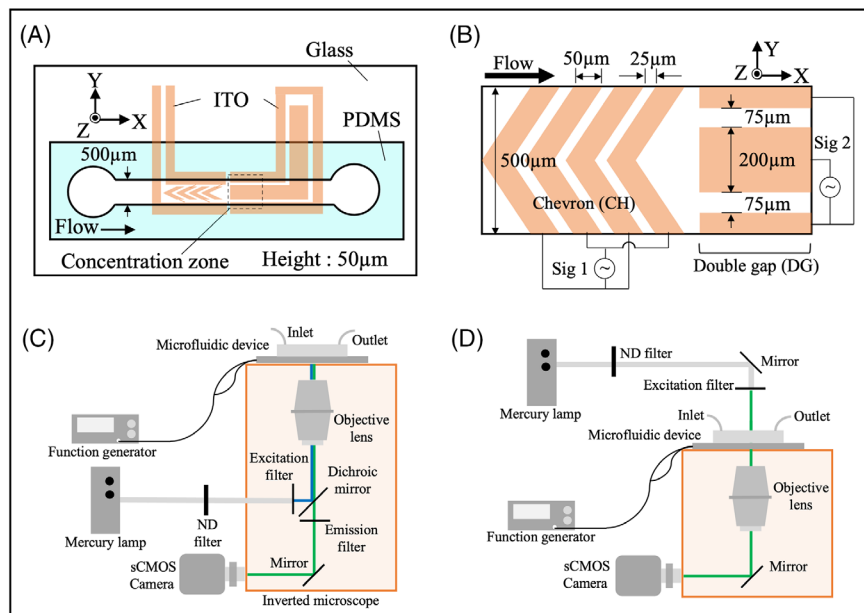


FIGURE 2 (A) Schematic of microfluidic particle concentrator. (B) Cascade design of the electrode: chevron (CH) and double gap (DG). The gap spacing in the CH pattern is 25 μm and 75 μm in the DG zone. In cascade ACEO (cACEO), CH is located 2 mm upstream of DG, connecting separate electric circuits. (C) Schematic of the experimental setup used to observe latex and liposome nanoparticle samples. (D) Schematic of the experimental setup used to observe metal nanoparticle samples

(ITO) electrode was used, which allows easy optical access through the substrate, because the ITO electrode is transparent and particle images can be observed using inverted microscopy. Sputtering was used to place the electrode on the glass, and a standard wet etching process was used for patterning.

The PDMS microchannel (Sylgard 184, Dow Corning Toray, Japan) was fabricated using standard soft lithography at 500 μm width, 50 μm height, and 50 mm length. The PDMS channel was attached to a 0.7-mm-thick glass substrate with a transparent ITO film electrode. Perfluoroalkoxy alkane tubes were connected at the inlet and outlet, and a pressure-driven flow was generated by a difference in the liquid surface levels between the inlet and outlet. The bulk velocity was set at <1 mm/s. A function generator (AFG3022B, Tektronix, USA) connected to the electrodes applied an AC electric field to the device with a voltage of 1.0–10.0 V_{pp} at a frequency of 0.1–1.0 kHz.

2.2 | Sample preparation and experimental method

To demonstrate the efficiency of cACEO in continuous concentration, we used three types of nanoparticles: latex, metal, and liposomes.

2.2.1 | Latex nanoparticles

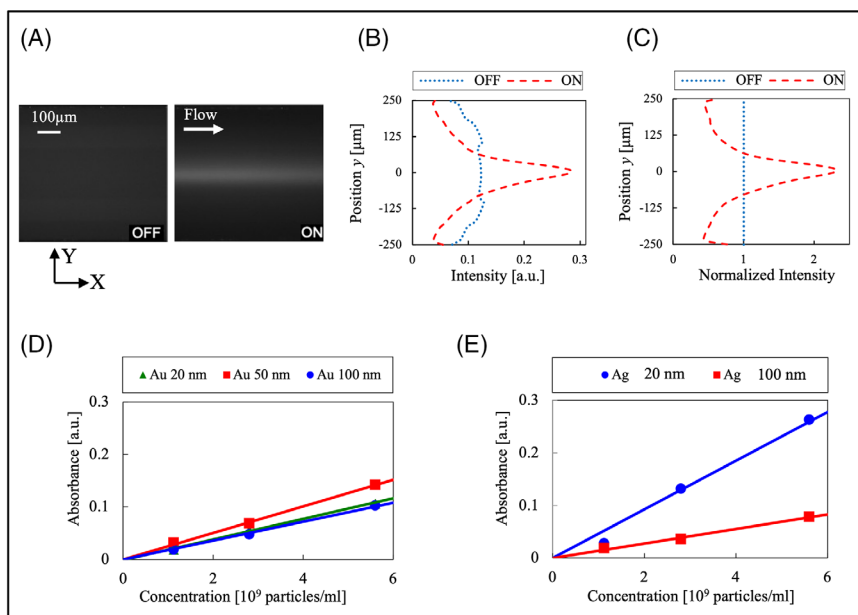
The first sample included latex nanoparticles, which was prepared using fluorescent polystyrene nanospheres (Flu-

oSpheres, Invitrogen, USA) with a diameter of 50 nm and dispersed in KCl aqueous solution (Wako Pure Chemical Industries, Japan). The fluorescent particles had excitation and emission wavelengths of 505 and 515 nm, respectively. The solution electrical conductivity was tuned to 4.4 mS/m. To avoid particle–particle interaction, particle volume in the working fluid was set to 0.01%. The fluorescent nanoparticle analysis employed in this work was mostly conducted for an image brightness analysis.

The behavior of polystyrene nanoparticles (PsNPs) was visualized using inverted microscopy. Figure 2C illustrates the experimental setup used for observing latex and liposome nanoparticle samples. A continuous mercury lamp (Intensilight C-HGFI, Nikon, Japan) was used as an illumination source. The filter cube with an exciter filter, an emitter filter, and a dichroic mirror, which are tailored for effective particle excitation and collection of fluorescent light, was included in the microscope. A scientific complementary metal oxide semiconductor (sCMOS) camera (ORCA-Flash2.8, Hamamatsu Photonics, Japan) was used to capture the images.

Figure 3A depicts the raw images of nanoparticle distribution inside a microchannel under two different conditions: voltage off and voltage on. The images were processed to obtain an average intensity value in the streamwise direction. Hypothetically, when the voltage is turned off, the particles and intensity should be evenly dispersed in the liquid. However, the intensity distribution was slightly inhomogeneous due to the nonuniformity of the illumination source and the low light absorption of the ITO electrode, as seen in Figure 3B. As illustrated in Figure 3C, a normalizing process was required to reduce

FIGURE 3 (A) Raw images of polystyrene nanoparticle (PsNP) distribution under different conditions: voltage off and voltage on. In the off case, intensity distribution is slightly inhomogeneous, due to the nonuniformity of the illumination source and the light absorption of the ITO electrode, as seen in (B). The normalization process reduced this effect, as shown in (C). The lower part of the figure indicates the calibration curve of absorbance as a function of concentration (particles/ml): (D) gold nanoparticles (AuNPs) with sizes of 20, 50, and 100 nm. (E) Silver nanoparticles (AgNPs) with sizes of 20 nm and 100 nm, obtained for $\lambda = 530$ nm for AuNPs and $\lambda = 410$ nm for AgNPs. The solid lines represent the best fit for the experimental data



this effect. The normalized fluorescence intensity indicates how much the particle concentration changes, which is defined as the concentration factor (CF). Here, the fluorescent intensity value distribution acquired before applying voltage was used for normalization.

2.2.2 | Metal nanoparticles

ACEO flow can also be used to organize metal nanoparticles. Gold nanoparticles (AuNPs) with diameters of 20, 50, and 100 nm were used in this study (EMGC 20, 50, and 100, BBI Solutions, USA). In addition, cases using silver nanoparticles (AgNPs) with diameters of 20 and 100 nm (Sigma-Aldrich, USA) were also investigated. These particles were also visualized by using inverted microscopy containing the above-described optical systems, except for the fluorescence filter, as shown in Figure 2D. Here, the surface plasmon resonance of metal nanoparticles due to strong light absorption in a particular wavelength was used to visualize and quantify particle concentration. Calibration curves of AuNPs and AgNPs in an aqueous solution were produced for each diameter using a spectrometer before the microfluidic experiments. Nanoparticle concentration distribution could be then visualized via illumination using the light with the corresponding absorption band. Figure 3D,E depicts the light absorbance behavior of AuNPs with diameters of 20, 50, and 100 nm, as well as AgNPs with sizes of 20 and 100 nm, at various sample concentrations. Regardless of particle size, AuNPs and AgNPs followed a similar pattern. As the number of parti-

cles in the sample rises, the ability to absorb light increases, appearing as a dark area in the image. Consequently, the brightness intensity distribution derived from the acquired images indicates the metal nanoparticle concentration distribution. Finally, we obtained a CF value using the same normalization procedure as for latex nanoparticles.

2.2.3 | Liposomes

Liposomes are biocompatible bilayered spherical containers that have been extensively used as a biological membrane model that imitates the lipid bilayer cell membrane. They are also used for drugs, peptides, proteins, plasmid DNA, or antisense oligonucleotides used in pharmaceutical, cosmetic, and biochemical applications [33]. In recent years, applications as drug delivery carriers and gene transfer systems have been actively studied using their ability to uptake substances into the internal aqueous phase. When liposomes are used as substance carriers, their membrane permeability is an important property, which requires elucidation of the properties of solvents, targets, and liposomes themselves. Maleic acid buffer (1 mM) with 5% ethanol was used as a solvent. Lipid concentration was adjusted to 0.125 mM, and 1% of the fluorescent dye was used. In this study, liposomes were colored with red fluorescent rhodamine-DOPE, and the excitation and emission wavelengths were 546 nm and 576 nm, respectively. Therefore, the fluorescent observation system mentioned in Section 2.2.1 was also used here to obtain the CF of liposomes in the microchannel.

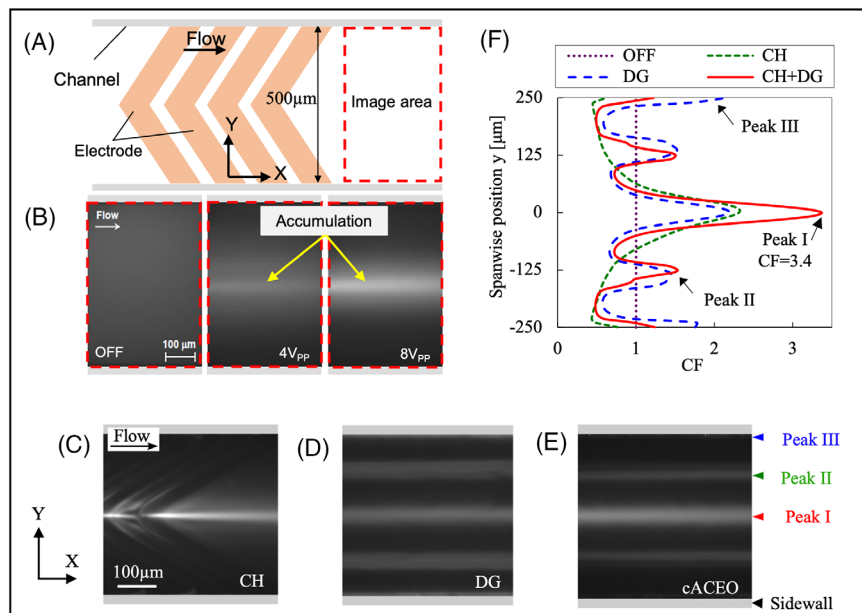


FIGURE 4 The upper left part indicates polystyrene nanoparticle (PsNP) accumulation behavior using the chevron (CH) electrode only. (A) The analysis area is indicated by a dashed rectangle. (B) Depth-average fluorescent intensity for PsNPs before applying a voltage at 4 V_{pp} and 8 V_{pp}. The lower part shows the concentration of 50 nm PsNPs. Depth-average fluorescence intensity for particle concentration using the CH (C), double-gap (DG) (D), and cascade alternating current electroosmosis (cACEO) electrodes (E). The concentration factor of PsNPs in the horizontal distribution in different electrode patterns is illustrated in (F)

3 | RESULTS AND DISCUSSION

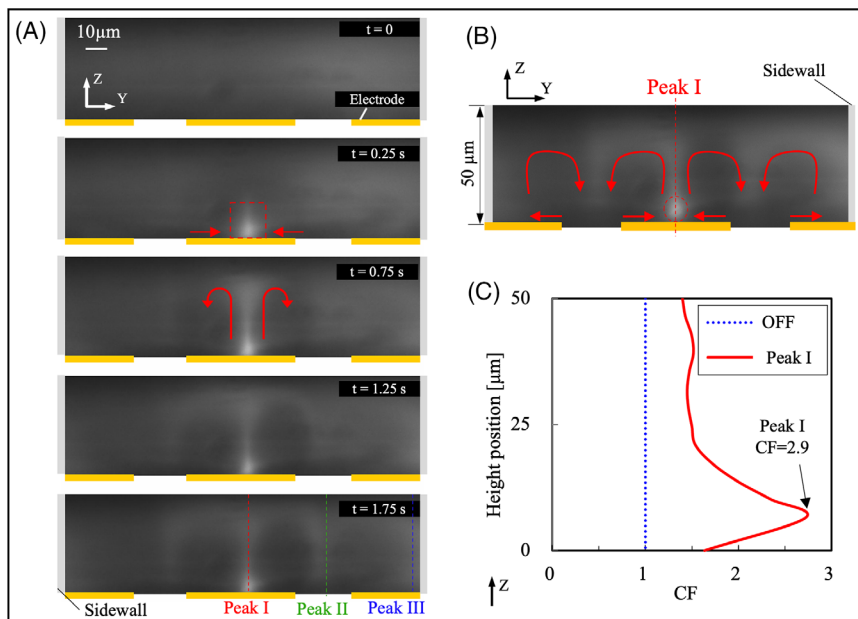
3.1 | Effective concentration of PsNPs

To demonstrate the feasibility of using cACEO in effective nanoparticle focusing, 50-nm PsNPs suspended in KCl aqueous solution with a conductivity of 4.4 mS/m were used as a benchmark. As mentioned in Section 2, CH branches generate inward flow from the sidewall to the center of the channel. To indicate the role of the CH electrode, an experiment for nanoparticle accumulation using only the CH electrode is conducted. The analysis area was set downstream of the CH electrode, as illustrated in Figure 4A. The experimental results shown in Figure 4B indicated a higher intensity in the center of the channels and lower intensity near the channel edge after applying voltage. Thus, the nanoparticles accumulated from the sidewall in the direction of the channel center. Figure 4C–E shows the accumulation behavior of nanoparticles in CH, DG, and cACEO electrodes, respectively. A voltage of 6 V_{pp} and a frequency of 100 Hz were applied to each electrode pattern separately. When using CH electrodes, PsNPs concentrated around the center of the channel, at the peak I position. Conversely, using DG electrodes enabled particles to concentrate at the center, at peak I, as well as at two intermediate regions, indicated as peak II. The peak III position near the sidewalls was attributed to the counter-ACEO flow. Particle behavior near the channel wall was described in detail in our related work [32]. To avoid particle flow in the scattering zone when using DG, the initial position of particles requires control. The CH electrode could induce ACEO flow to collect particles from the sidewall region to the center region to promote DG

concentration function. Therefore, the combined mode was utilized by applying the same signal to each electrode simultaneously. A higher fluorescence intensity appeared at peak I. A comparison between the CF values of each electrode pattern, CH, DG, and the combined pattern, is shown in Figure 4F. The number of focused nanoparticles, at the channel center, was much higher under cACEO than that under DG alone. The intensity value near the sidewall decreased significantly, compared with DG. Most nanoparticles passing the entire spanwise area in the channel were collected near the center area by the flow induced by CH electrodes. Consequently, the CF value in cACEO reached 3.4. This shows an improvement in particle concentration of 62%, compared with the use of DG electrodes alone. The FWHM of concentrated nanoparticle distribution in the cascade device was approximately 61 μm, equal to 12.2% of the channel width.

ACEO generates a 3D flow transporting suspended particles to a certain location on the electrode surface depending on electric field strength [34]. ACEO induced around CH effectively concentrated particles to the center of the channel, and induction around DG concentrated particles to the electrode surface. However, as shown in Figure 4E, high-intensity areas appeared far from the center of the channel, indicated as peak II. For further understanding, nanoparticle concentration was observed from the cross-sectional direction of the microchannel. To investigate the cross-sectional phenomenon and clarify the source of peak II, this experiment was performed using a stationary fluid over a DG electrode. Furthermore, wider space for the accumulation is given in the middle electrode and smaller double-gap is used. Here, the middle electrode width was 300 μm and each gap

FIGURE 5 (A) Successive cross-sectional images of fluorescent polystyrene nanoparticle (PsNP) concentration profiles using cascade alternating current electroosmosis (cACEO) under an applied voltage of $6 V_{pp}$ and a frequency of 100 Hz at $t = 0, 0.25, 0.75, 1.25$ and 1.75 s. (B) Cross-sectional view of fluorescent nanoparticle distribution under cACEO, arrows show the movement of the nanoparticles under the applied voltage. (B) Intensity distribution at the stagnation point, Peak I



width was 25 μm . The cross-sectional images of the fluorescence intensity profile depicting the temporal change in nanoparticle behavior after applying voltage are shown in Figure 5A. These images were acquired downstream of DG electrodes. These visualized images demonstrate that the majority of nanoparticles suspended in the solution could be focused in 3D on the surface area. The ACEO transported particles to the stagnation point, bounded by the dashed square at $t = 0.25$ s. After blowing up to the upper section of the flow path at $t = 0.75$ s, nanoparticles flowed in a ring shape into the gap at the electrode surface at $t = 1.25$ and 1.75 s. Simultaneously, there was a dense area of nanoparticles near each sidewall region, which can be attributed to the counter-ACEO flow, as illustrated in Figure 5B. This flow forms a peak at the gap when observed downward, as shown in Figure 4E. Additionally, CF distribution in the height direction acquired at the center of the channel is shown in Figure 5C. The CF value in terms of height of the channel at the peak I position was around 2.9.

3.2 | AuNP and AgNP focusing

Subsequently, to demonstrate the versatility of the proposed device, we also investigated the efficiency of metal nanoparticle focusing. Figure 6A, obtained in the DG section, shows 50-nm AuNPs with an applied voltage of $8 V_{pp}$. When an electric field is introduced, accumulated nanoparticles can be seen as a black region, highlighted by a dashed rectangle in the image ("ON" in Figure 6A). Figure 6B shows the CF for 50-nm AuNPs in the cACEO device after applying an AC electric field at

2, 4, and 6 V_{pp} . Here, a brightness intensity was evaluated downstream of the DG electrode section. The range where sufficient absorption was observed for CF calculation was about 20 μm wide, which is almost the same as the width of the region where the CF of fluorescent PsNPs was ≥ 3 . The FWHM of concentrated AuNP distribution in the cascade device was approximately 7 μm , equal to 1.4% of the channel width. Thus, it is more difficult to obtain the CF distribution of AuNPs than that of the fluorescent particles. Therefore, we selected appropriate working conditions, such as voltage, to increase the ACEO velocity and improve observation. Here, experiments were conducted in the range of 4–10 V_{pp} , considering electrode durability and function generator stability.

The size-dependent CF of the metal nanoparticles was calculated based on the corresponding calibration curves. The CF showed a positive dependence on both the applied voltage and the particle size. Figure 6C shows the CF of the metal nanoparticles at different applied voltages. AuNPs with a particle size of 100 nm and AgNPs with a particle size of 100 nm had almost identical CF, and it could be said that the effect of particle type on CF was very small. On contrary, for 100 nm particles with 10 V_{pp} , CF reached almost 67. The 20-nm AgNPs exhibited the same tendency, that is, higher CF at higher voltages, in the introduced voltage range. At a voltage of 10 V_{pp} , the CF reached 20.

3.3 | Liposome concentration

Figure 7A shows the results of liposome enrichment. The applied voltage was 12 V_{pp} , and the frequency was

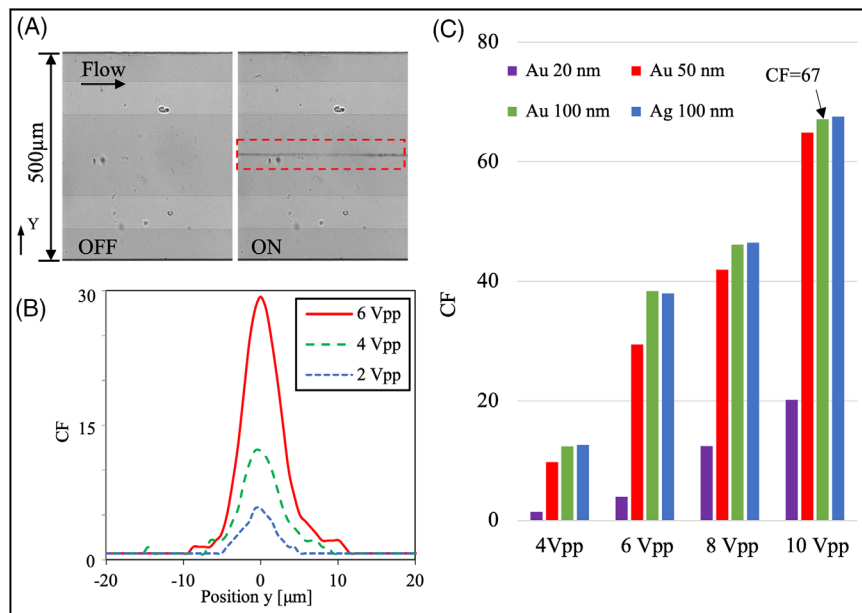


FIGURE 6 (A) Concentration of gold nanoparticles (AuNPs) (50 nm) at the double-gap (DG) electrode. Nanoparticles are visualized using light absorption due to surface plasmon resonance. (B) Concentration factor of AuNPs (50 nm) in the cascade concentration device at different voltages. (C) Concentration factors of AuNPs and silver nanoparticles (AgNPs) with sizes ranging from 20 to 100 nm

0.5 kHz. As liposome particle size was mostly around 50 nm, they could be treated similarly as fluorescent PsNPs. Unlike other particles, maleic acid buffer containing 5% ethanol was used as the solvent, and the conductivity was 9.3 mS/m. Figure 7B shows the CF of the liposomes. Since the conductivity of liposomes solution is higher than that of the aforementioned conductivity of PsNPs, and the high conductivity leads to better ion dissipation that results in weak ACEO flow, the CF of liposomes was lower than that of PsNPs. The FWHM of concentrated nanoparticle distribution in the cascade device was approximately 26 μm , equal to 5.2% of the channel width. Although the CF value was low, it increased significantly > 1 , which is substantial for all intents and purposes. As a consequence, we were able to demonstrate that the devised device is effective in concentrating biomaterials.

4 | CONCLUDING REMARKS

In this article, an effective method for continuous nanoparticle concentration using cACEO was introduced. The position where nanoparticles accumulate could be controlled by the electrode pattern. Especially, the particles in the scattering area were accumulated around the center of the channel by using CH electrodes; then, further concentration could be achieved using DG electrodes. The experimental results showed that the proposed device was effective in concentrating nanoparticles regardless of particle size or electrical properties. The cACEO device generates both horizontal and vertical concentrations on

the electrode surface at the center of the channel. Using fluorescent PsNPs, the CF reached 3.4 when the concentrated nanoparticles were distributed in 12.2% of the channel width. In the case of metal nanoparticles, a highly efficient concentration performance for AuNPs with a CF of 67 was confirmed. The AuNPs accumulated within 7 μm , which represents 1.4% of the channel width. In addition, cACEO was utilized to accumulate biomaterials, namely liposomes, to demonstrate its efficiency. Although liposome concentration and results were not as good as fluorescent PsNPs because the fluorescence intensity of the liposomes was low, the CF value reached > 1 . Therefore, cACEO can be applied for biomaterial accumulation. Although there are many opportunities to refine and optimize electrode shape and characteristics for target nanomaterials, as we used the same device for all experiments, the cACEO concentrator holds significant potential to concentrate nanoscale samples, such as particles, rare samples, and biomaterials.

ACKNOWLEDGMENTS

A part of this research was financially supported by Japan Society for the Promotion of Science (JSPS) KAKENHI Grant No. 19H02084 and 19K21936. A part of the microfabrication was partially supported by the Advanced Research Infrastructure for Materials and Nanotechnology (ARIM), supported by the Ministry of Education, Culture, Sports, Science, and Technology (MEXT), Japan.

CONFLICT OF INTEREST

The authors have declared no conflict of interest.

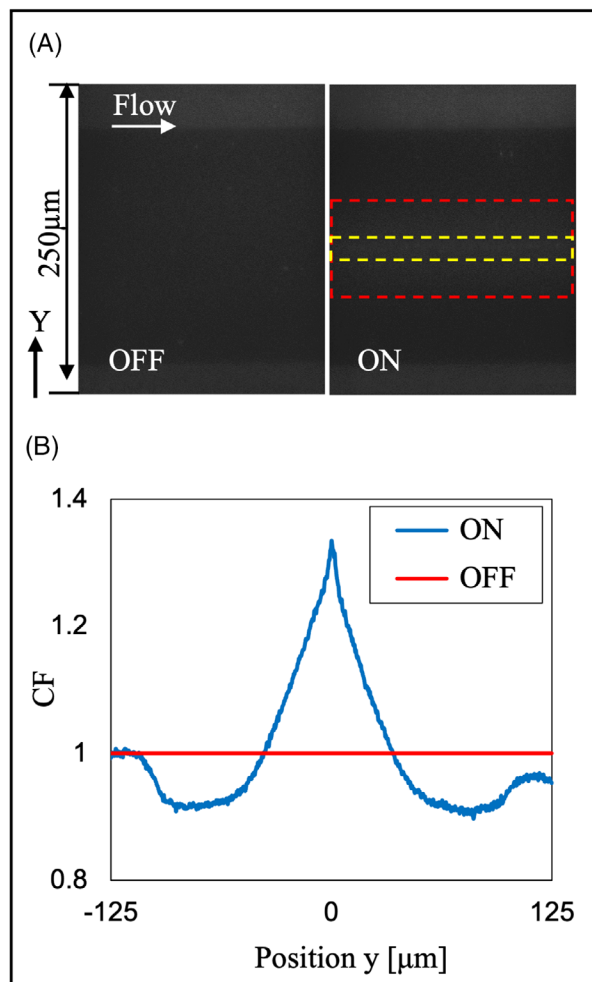



FIGURE 7 (A) Fluorescent images of liposome nanoparticles in a cascade concentration device with and without voltage applied. Concentration factor >1 is represented by the region in the outer dashed rectangle (red), and concentration factor >1.2 is represented by the area in the inner dashed rectangular (yellow). (B) The fluorescence intensity profile of liposome nanoparticles indicates the concentration value in the cascade device

DATA AVAILABILITY STATEMENT

Data underlying the results presented in this paper are not publicly available at this time but may be obtained from the authors upon reasonable request.

ORCID

Ahmed Abdelghany  <https://orcid.org/0000-0002-2558-030X>

Yoshiyasu Ichikawa  <https://orcid.org/0000-0002-5615-7002>

Masahiro Motosuke  <https://orcid.org/0000-0001-6961-0382>

REFERENCES

1. Yeo LY, Chang HC, Chan PPY, Friend JR. Microfluidic devices for bioapplications. *Small*. 2011;7(1):12–48.
2. Neethirajan S, Kobayashi I, Nakajima M, Wu D, Nandagopal S, Lin F. Microfluidics for food, agriculture and biosystems industries. *Lab Chip*. 2011;11(9):1574–86.
3. Whitesides GM. The origins and the future of microfluidics. *Nature*. 2006;442(7101):368–73.
4. Hu M, Yan J, He Y, Lu H, Weng L, Song S, et al. Ultrasensitive, multiplexed detection of cancer biomarkers directly in serum by using a quantum dot-based microfluidic protein chip. *ACS Nano*. 2010;4(1):488–94.
5. Lin CC, Hsu JL, Lee GB. Sample preconcentration in microfluidic devices. *Microfluid Nanofluid*. 2011;10(3):481–511.
6. Di Carlo D, Irimia D, Tompkins RG, Toner M. Continuous inertial focusing, ordering, and separation of particles in microchannels. *Proc Natl Acad Sci USA*. 2007;104(48):18892–7.
7. Nilsson A, Petersson F, Jönsson H, Laurell T. Acoustic control of suspended particles in micro fluidic chips. *Lab Chip*. 2004;4(2):131–5.
8. Shi J, Yazdi S, Lin SCS, Ding X, Chiang IK, Sharp K, et al. Three-dimensional continuous particle focusing in a microfluidic channel via standing surface acoustic waves (SSAW). *Lab Chip*. 2011;11(14):2319–24.
9. Liu Y, Edmond KV, Curran A, Bryant C, Peng B, Aarts DGAL, et al. Core-shell particles for simultaneous 3D imaging and optical tweezing in dense colloidal materials. *Adv Mater*. 2016;28(36):8001–6.
10. García-Arribas A, Martínez F, Fernández E, Ozaeta I, Kuryandskaya GV, Svalov AV, et al. GMI detection of magnetic-particle concentration in continuous flow. *Sens Actuators A*. 2011;172(1):103–8.
11. Holmes D, Morgan H, Green NG. High throughput particle analysis: combining dielectrophoretic particle focussing with confocal optical detection. *Biosens Bioelectron*. 2006;21(8):1621–30.
12. Yu C, Vykoukal J, Vykoukal DM, Schwartz JA, Shi L, Gascoyne PRC. A three-dimensional dielectrophoretic particle focusing channel for microcytometry applications. *J Microelectromech Syst*. 2005;14(3):480–7.
13. Chu H, Doh I, Cho YH. A three-dimensional (3D) particle focusing channel using the positive dielectrophoresis (pDEP) guided by a dielectric structure between two planar electrodes. *Lab Chip*. 2009;9(5):686–91.
14. Zhu J, Tzeng TRJ, Hu G, Xuan X. DC dielectrophoretic focusing of particles in a serpentine microchannel. *Microfluid Nanofluid*. 2009;7(6):751.
15. Salemmilani R, Piorek BD, Mirsafavi RY, Fountain AW, III, Moskovits M, Meinhart CD. Dielectrophoretic nanoparticle aggregation for on-demand surface enhanced raman spectroscopy analysis. *Anal Chem*. 2018;90(13):7930–6.
16. Jia Y, Ren Y, Jiang H. Continuous-flow focusing of microparticles using induced-charge electroosmosis in a microfluidic device with 3D AgPDMS electrodes. *RSC Adv*. 2015;5(82):66602–10.
17. Liu W, Tao Y, Xue R, Song C, Wu Q, Ren Y. Continuous-flow nanoparticle trapping driven by hybrid electrokinetics in microfluidics. *Electrophoresis*. 2021;42(7–8):939–49.

18. Tao Y, Ren Y, Liu W, Wu Y, Jia Y, Lang Q, et al. Enhanced particle trapping performance of induced charge electroosmosis. *Electrophoresis*. 2016;37(10):1326–36.
19. Mohtar MN, Hoettges KF, Hughes MP. Factors affecting particle collection by electro-osmosis in microfluidic systems. *Electrophoresis*. 2014;35(2–3):345–51.
20. Hoettges KF, McDonnell MB, Hughes MP. Continuous flow nanoparticle concentration using alternating current-electroosmotic flow. *Electrophoresis*. 2014;35(4):467–73.
21. Liu W, Ren Y, Tao Y, Zhou Z, Wu Q, Xue R, et al. Multiple frequency electrothermal induced flow: theory and microfluidic applications. *J Phys D Appl Phys*. 2020;53(17):175304.
22. Hossan MR, Dutta D, Islam N, Dutta P. Review: electric field driven pumping in microfluidic device. *Electrophoresis*. 2018;39(5–6):702–31.
23. Liu W, Ren Y, Xue R, Song C, Wu Q. On ion transport regulation with field-effect nonlinear electroosmosis control in microfluidics embedding an ion-selective medium. *Electrophoresis*. 2020;41(10–11):778–92.
24. Ramos A, Morgan H, Green NG, Castellanos A. AC electrokinetics: a review of forces in microelectrode structures. *J Phys D Appl Phys*. 1998;31(18):2338.
25. Jubery TZ, Srivastava SK, Dutta P. Dielectrophoretic separation of bioparticles in microdevices: a review. *Electrophoresis*. 2014;35(5):691–713.
26. Pethig R. Dielectrophoresis: status of the theory, technology, and applications. *Biomicrofluidics*. 2010;4(2):22811.
27. Wu J, Ben Y, Battigelli D, Chang HC. Long-range AC electroosmotic trapping and detection of bioparticles. *Ind Eng Chem Res*. 2005;44(8):2815–22.
28. Bhatt KH, Grego S, Velev OD. An AC electrokinetic technique for collection and concentration of particles and cells on patterned electrodes. *Langmuir*. 2005;21(14):6603–12.
29. Melvin EM, Moore BR, Gilchrist KH, Grego S, Velev OD. On-chip collection of particles and cells by AC electroosmotic pumping and dielectrophoresis using asymmetric microelectrodes. *Biomicrofluidics*. 2011;5(3):34113–3411317.
30. Castellanos A, Ramos A, González A, Green NG, Morgan H. Electrohydrodynamics and dielectrophoresis in microsystems: scaling laws. *J Phys D Appl Phys*. 2003;36(20):2584–97.
31. Lian M, Islam N, Wu J. Particle line assembly/patterning by microfluidic AC electroosmosis. *J Phys Conf Series*. 2006;34:589.
32. Motosuke M, Yamasaki K, Ishida A, Toki H, Honami S. Improved particle concentration by cascade AC electroosmotic flow. *Microfluid Nanofluid*. 2013;14(6):1021–30.
33. Ulrich AS. Biophysical aspects of using liposomes as delivery vehicles. *Biosci Rep*. 2002;22(2):129–50.
34. Ramos A, Morgan H, Green NG, Castellanos A. AC electric-field-induced fluid flow in microelectrodes. *J Colloid Interface Sci*. 1999;217(2):420–2.

How to cite this article: Abdelghany A, Yamasaki K, Ichikawa Y, Motosuke M. Efficient nanoparticle focusing utilizing cascade AC electroosmotic flow. *Electrophoresis*. 2022;43:1755–1764.
<https://doi.org/10.1002/elps.202200054>